Original Article

Blockers of the Delayed-Rectifier Potassium Current in Pancreatic β-Cells Enhance Glucose-Dependent Insulin Secretion

James Herrington,[1] Yun-Ping Zhou,[2] Randal M. Bugianesi,[1] Paula M. Dulski,[1] Yue Feng,[2] Vivien A. Warren,[1] McHardy M. Smith,[1] Martin G. Kohler,[1] Victor M. Garsky,[3] Manuel Sanchez,[4] Michael Wagner,[1] Kristin Raphaelli,[1] Priya Banerjee,[1] Chinweze Ahaghotu,[1] Denise Wunderler,[1] Birgit T. Priest,[1] John T. Mehl,[5] Maria L. Garcia,[1] Owen B. McManus,[1] Gregory J. Kaczorowski,[1] and Robert S. Slaughter[1]

Downloaded from http://diabetesjournals.org/diabetes/article-pdf/55/4/1034/383688/zdb00406001034.pdf by guest on 24 February 2022

Delayed-rectifier K^+ currents (I_{DR}) in pancreatic β-cells are thought to contribute to action potential repolarization and thereby modulate insulin secretion. The voltage-gated K^+ channel, $K_V2.1$, is expressed in β-cells, and the biophysical characteristics of heterologously expressed channels are similar to those of I_{DR} in rodent β-cells. A novel peptidyl inhibitor of $K_V2.1/K_V2.2$ channels, guangxitoxin (GxTX)-1 (half-maximal concentration ~1 nmol/l), has been purified, characterized, and used to probe the contribution of these channels to β-cell physiology. In mouse β-cells, GxTX-1 inhibits 90% of I_{DR} and, as for $K_V2.1$, shifts the voltage dependence of channel activation to more depolarized potentials, a characteristic of gating-modifier peptides. GxTX-1 broadens the β-cell action potential, enhances glucose-stimulated intracellular calcium oscillations, and enhances insulin secretion from mouse pancreatic islets in a glucose-dependent manner. These data point to a mechanism for specific enhancement of glucose-dependent insulin secretion by applying blockers of the β-cell I_{DR}, which may provide advantages over currently used therapies for the treatment of type 2 diabetes. *Diabetes* 55: 1034–1042, 2006

Insulin secretion from pancreatic β-cells in response to glucose is regulated by ATP-sensitive K^+ channel (K_{ATP} channel) and by K_{ATP} channel–independent pathways (1). In the K_{ATP} channel–dependent pathway, changes in cellular ATP/ADP levels brought about by the metabolism of glucose cause closure of K_{ATP} channels, which sets the resting membrane potential of these cells. The closure of K_{ATP} channels leads to depolarization of the plasma membrane, opening of voltage-gated calcium channels, and an increase in cytosolic free calcium, $[Ca^{2+}]_i$, to trigger insulin secretion (2). Sulfonylureas, the current first-line treatment in type 2 diabetes, block K_{ATP} channels to induce insulin secretion, but because the action of sulfonylureas is not glucose dependent, patients often exhibit episodes of hypoglycemia (3).

In addition to K_{ATP} channels, several other types of K^+ channels are present in β-cells, such as large-conductance calcium-activated K^+ channel (4), a voltage-independent calcium-activated K^+ channel (5,6), and a rapidly inactivating voltage-gated K^+ channel (7,8).

The delayed-rectifier K^+ current (I_{DR}) is prominent in β-cells from several species, including humans (9), and is thought to contribute to repolarization of action potentials (10). Inhibition of I_{DR} should broaden action potentials, raise intracellular calcium levels, and enhance insulin secretion in a glucose-dependent manner (8,11,12). For these reasons, the β-cell I_{DR} has been considered a potential target for the development of novel agents for treatment of type 2 diabetes (13), although its molecular identity remains to be defined.

Of the K_V channel subtypes that have been reported to be expressed in islet tissue, $K_V2.1$ is prominent in β-cells and exhibits biophysical properties similar to the β-cell I_{DR} (13). A $K_V2.1$ dominant-negative construct reduced β-cell I_{DR} and enhanced glucose-stimulated insulin secretion (GSIS) (8). In addition, hanatoxin (HaTX), a peptidyl $K_V2.1$ inhibitor, has been reported to enhance GSIS (14) and to induce calcium oscillations in mouse and human islets (15). Lack of commercial availability of HaTX has hindered further studies on the mechanism of reported effects on GSIS.

To probe the role of I_{DR} in β-cells, a novel peptide inhibitor, guangxitoxin (GxTX)-1, was purified to homogeneity and synthetically produced. This peptide is a potent inhibitor of $K_V2.1/K_V2.2$ channels and inhibits most of I_{DR} in mouse β-cells. GxTX-1 broadens the β-cell action potential, enhances calcium oscillations, and augments GSIS but has no effect on secretion under low-glucose conditions. These data suggest that $K_V2.1$ is a component of I_{DR}

From the [1]Department of Ion Channels, Merck Research Laboratories, Rahway, New Jersey; the [2]Department of Metabolic Disorders–Diabetes, Merck Research Laboratories, Rahway, New Jersey; the [3]Department of Medicinal Chemistry, Merck Research Laboratories, West Point, Pennsylvania; the [4]Department of Farmacologia, Universidad de Oviedo, Oviedo, Spain; and the [5]Department of Drug Metabolism, Merck Research Laboratories, West Point, Pennsylvania.

Address correspondence and reprint requests to James Herrington, Merck Research Laboratories, RY80N-C31, P.O. Box 2000, Rahway, NJ 07065-0900. E-mail: james_herrington@merck.com.

Received for publication 21 June 2005 and accepted in revised form 21 December 2005.

J.H. and Y.-P.Z. contributed equally to this article.

GSIS, glucose-stimulated insulin secretion; GxTX, guangxitoxin; HaTX, hanatoxin; HPLC, high-performance liquid chromatography; I_{DR}, delayed-rectifier K^+ currents; K_{ATP} channel, ATP-sensitive K^+ channel; KRB, Krebs-Ringer bicarbonate; TFA, trifluoroacetic acid.

© 2006 by the American Diabetes Association.

The costs of publication of this article were defrayed in part by the payment of page charges. This article must therefore be hereby marked "advertisement" in accordance with 18 U.S.C. Section 1734 solely to indicate this fact.

TABLE 1
Sequence homology

Peptide	Sequence	Amino acid identity to GxTX-1E	Channel activity
GxTX-1E	EGECGGFWWKCGSGKPACC--PKYVCSPKW--GLCNFPMP-	36	K_V2.1 K_V2.2 K_V4.3
GxTX-1D	DGECGGFWWKCGSGKPACC--PKYVCSPKW--GLCNFPMP-	35	K_V2.1
Jingzhaotoxin-III	DGECGGFWWKCGRGKPPCC--KGYACSKTW--GWCAVEAP-	22	Cardiac TTXr
GsMTx-4	--GCLEFWWKCNPNDDKCCR-PKLKCSKLF--KLCNFSF-	16	Stretch channel
VSTX1	--ECGKFMWKCKN-SNDCCK--DLVCSSRW--KWCVLPAPW	15	K_VAP
Hainantoxin-III	--GCKGFGDSCTPGKNECC--PNYACSSKH--KWCKVYL--	14	DRG Na_V 1 nmol/l
Huwentoxin-I	--ACKGVFDACTPGKNECC--PNRVCSDKH--KWCVLASPF	14	Ca_V2.2 100 nmol/l
Hainantoxin-I	--ECKGFGKSCVPGKNECC--SGYACNSRD--KWCKVLL--	12	Na_V1.2 TTXs not DRG Na_V
Hainantoxin-IV	--ECLGFGKGCNPSNDQCCKSSNLVCSRKH--RWCKYEI--	12	DRG Na_V 45 nmol/l
ω-GsTx SIA	--DCVRFWGKC-SQTSDCC--PHLACKSKWPRNICVWDGSV	11	Nerve Ca_V
GxTX-2	--ECRKMFGGC-SVDSDCC--AHLGCKPTL--KYCAWDGT	9	K_V2.1
ScTx1	--DCTRMFGAC-RRDSDCC--PHLGCKPTS--KYCAWDGT	8	K_V2.1 K_V2.2 K_V2.1/9.3 K_V4.2
Hanatoxin	--ECRYLFGGC-KTTSDCC--KHLGCKFRD-- C	7	K_V2.1
SGTx	--TCRYLFGGC-KTTSDCC--KHLACRSDG--KYCAWDGTF	6	K_V2.1

Residues that are indentical to GxTX-1E are shaded in gray. Cysteines are shown in dark gray. DRG, dorsal root ganglion; TTXr, tetrodotoxin resistant.

in β-cells and that I_{DR} represents an attractive target for the treatment of type 2 diabetes.

RESEARCH DESIGN AND METHODS

GxTX-1 purification. Aliquots of *Plesiophrictus guangxiensis* sp. nov. (16) venom (Spider Pharm, Yarnell, AZ), up to 300 μl original venom volume, were reconstituted with 10 vol of 20 mmol/l ammonium acetate, pH 6.2, and loaded onto a Brownlee CX-300 column pre-equilibrated with the same buffer at 1 ml/min. The column was developed using distilled deionized water as solvent A and 1 mol/l ammonium acetate at pH 6.2 as solvent B, using a gradient of 1.73% B/min. Absorbance at 280 nm was monitored, and peak fractions were collected, lyophilized, reconstituted in 140 mmol/l NaCl and 5 mmol/l HEPES-K, pH 7.4, and assayed for inhibition of K_V2.1 channel activity (see below). Selected fractions were pooled and subjected to reverse-phase high-performance liquid chromatography (HPLC) (C8, 4.6 × 250 mm; Vydac, Hesperia, CA) using 0.1% heptafluorobutyric acid in water (solvent A) and 0.1% heptafluorobutyric acid in 95% acetonitrile:water (solvent B) with a gradient of 10–50% B over 46 min at 1.25 ml/min. Absorbance was monitored at 220 nm. The third-stage C4 column (4.6 × 250 mm; Vydac) was developed with 10 mmol/l trifluoroacetic acid (TFA) in water (solvent A) and 9 mmol/l TFA in 95% isopropanol:5% water (solvent B). Active fractions were pooled, injected at 10% B, and eluted with a gradient of 10–50% B over 51 min at 1.0 ml/min. Absorbance was monitored at 210 nm. After lyophilization, active fractions were pooled and loaded onto a C18 column (4.6 × 250 mm; Vydac) with 10 mmol/l TFA in water as solvent A and 9 mmol/l TFA in 95% acetonitrile:water as solvent B. Material was eluted with a gradient of 20–50% B over 56 min at 1.0 ml/min, and absorbance at 210 nm was monitored. Active material eluting from this column was subjected to amino acid sequencing and mass spectrometry (17).

Peptide synthesis. GxTX-1E and GxTX-1D were synthesized (~0.5 mmol) by solid-phase methodology using a Boc protection strategy (18). Refolding of HPLC-purified hexahydro-peptides was achieved by air oxidation (0.1 mg/ml) in 2 mol/l urea, 0.1 mol/l Tris, pH 8.0, 0.15 mmol/l reduced glutathione, and 0.30 mmol/l oxidized glutathione. Folding and overall yields were 30 and 3.8% and 42 and 11.7% for GxTX-1E and GxTX-1D, respectively. The extinction coefficient for GxTX-1E determined from the synthetic material was within 10% of the value calculated from the sequence-based estimates from http://www.expasy.org/cgi-bin/protparam and http://www.basic.nwu.edu/biotools/proteincalc.html (19,20) (average, 18,890 at 280 nm). This extinction coefficient was used to determine the concentration of native GxTX-1.

K_V2.1 $^{86}Rb^+$ efflux assay. CHO.K_V2.1 cells (21) were loaded with 3.0 μCi/ml $^{86}Rb^+$ (Perkin Elmer), plated into 96-well microplates, and incubated overnight at 37°C. Wells were washed three times with Low K Buffer (in mmol/l, 135 NaCl, 5 KCl, 1 $CaCl_2$, 2 $MgCl_2$, and 10 HEPES, pH 7.4, with Tris), and 200 μl test compound in Low K Buffer plus 0.1% BSA was added to each well. After incubation at 22–24°C for 30 min, 200 μl High K Buffer (in mmol/l, 140 KCl, 1 $CaCl_2$, 2 $MgCl_2$, and 10 HEPES, pH 7.4, with Tris) plus 0.1% BSA in the presence of test compound was added, and incubation proceeded for additional 10 min. $^{86}Rb^+$ efflux was quantitated as previously described (21).

Patch-clamp electrophysiology. Membrane currents were recorded at room temperature (23–25°C) using standard dialyzed, whole-cell voltage clamp techniques (22) as described previously (9). From a holding potential of −80 mV, currents were activated by step depolarizations to potentials defined in the figures. For perforated-patch current clamp measurement of membrane potential, pipettes were filled with a solution containing (in mmol/l) 76 K_2SO_4, 10 KCl, 10 NaCl, 1 $MgCl_2$, and 5 HEPES, pH adjusted to 7.2, with KOH and backfilled with this solution supplemented with 0.24 mg/ml amphotericin B. The external solution was (in mmol/l) 140 NaCl, 3.6 KCl, 2 $NaHCO_3$, 0.5 NaH_2PO_4, 2.6 $CaCl_2$, 0.5 $MgSO_4$, and 5 HEPES, pH 7.4, with NaOH and supplemented with 0–15 mmol/l glucose as indicated. BSA (0.1% wt:vol) was added to GxTX-1 solutions.

***Xenopus* oocyte electrophysiology.** *Xenopus laevis* oocytes were prepared and injected with RNA encoding hK_V2.1, and currents were recorded using two-electrode voltage clamp as described previously (21,23).

IonWorks 384-well automated electrophysiology. K_V currents were recorded using the IonWorks HT system (Molecular Devices, Sunnyvale, CA) as described previously (21,24). Currents were measured before and 10 min after the addition of GxTX-1E in D-PBS containing 0.03% BSA. Peak currents at 0 mV (hK_V2.1) or +20 mV (hK_V2.2 and hK_V4.3) were analyzed as described below.

Analysis of electrophysiological data. The dose-dependence of tetraethylammonium inhibition of currents was determined from fits of the Hill equation, as described (9). The dose dependence of GxTX-1E inhibition was described by a single-site or a four-equivalent-site model with the equation $\rho_0 = (1 - p)^n$, where ρ_0 is the probability of the channel having zero GxTX-1E molecules bound, $p = [GxTX\text{-}1E]/([GxTX\text{-}1E] + K_D)$, and $n = 1$ or 4, respectively (25).

Fura-2 imaging. Dissociated mouse islet cells on glass coverslips were loaded with fura-2 AM (2 μmol/l) and imaged with a Nikon TE300 inverted microscope equipped with a Hamamatsu Orca-ER digital camera and a Lambda DG4 filter changer. Fura-2 was excited at 340 and 380 nm, fluorescence emission at 510 ± 20 nm was imaged every 10 s, and the average fluorescence intensity ratio (R) in a cell (F_{340}/F_{380}) was measured over time. To quantify changes in R, area under the curve was measured for 15 min before and 15 min after the addition of GxTX-1E or vehicle and percentage change calculated.

Islet isolation. Pancreatic islets of Langerhans were isolated from the pancreata of 8- to 14-week-old C57/B6 mice (Charles River, Wilmington, MA) by collagenase digestion and discontinuous Ficoll gradient separation, a modification of the original method of Lacy and Kostianovsky (26). The islets were cultured overnight in RPMI-1640 medium (11 mmol/l glucose) before experimental treatment.

Measurement of GSIS. GSIS was determined either by static incubation or perifusion of islets in Krebs-Ringer bicarbonate (KRB) medium at 37°C as described (27). For static GSIS assays, incubation was performed with

Downloaded from http://diabetesjournals.org/diabetes/article-pdf/55/4/1034/383688/zdb00406001034.pdf by guest on 24 February 2022

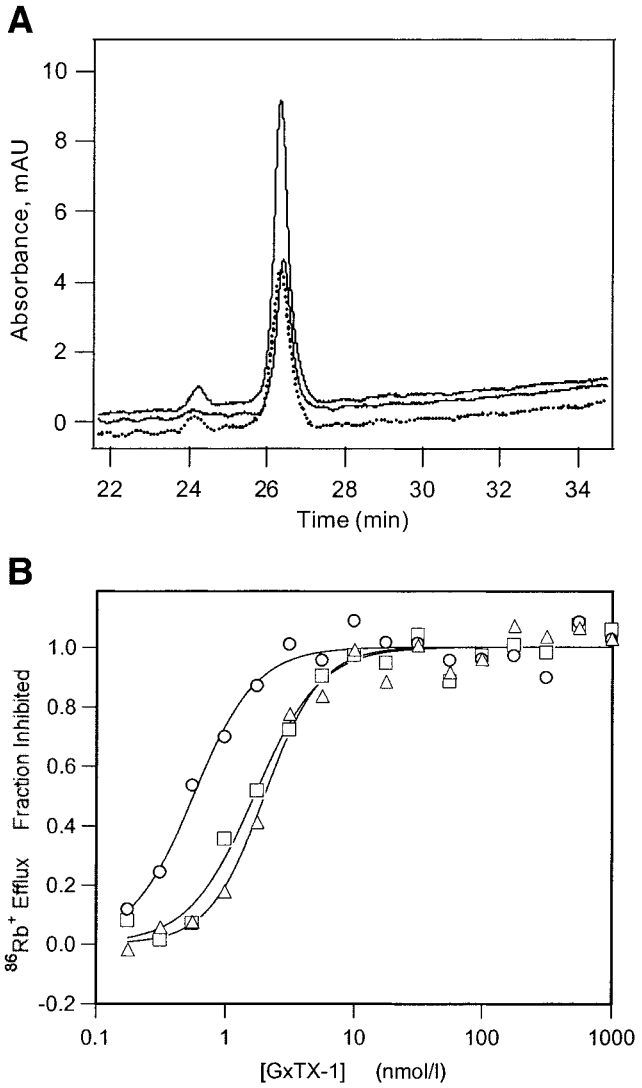

FIG. 1. Synthetic and native GxTX-1. *A*: Coelution. Synthetic GxTX-1E (middle solid trace), native GxTX-1 (bottom stippled trace), or combined synthetic and native (upper solid trace) were separated by reverse-phase HPLC. *B*: Inhibition of $^{86}Rb^+$ efflux through $K_V2.1$ by synthetic GxTX-1D (□), synthetic GxTX-1E (○), or native GxTX-1 (△). IC_{50}s for GxTX-1D, GxTX-1E, and native GxTX-1 were 1.7, 0.6, and 2.0 nmol/l, respectively.

round-bottomed 96-well plates (1 islet/well with 200 μl KRB medium). K_{ATP} channel–independent GSIS was measured by a modified static assay where, following a 30-min preincubation in unmodified KRB medium, islets were incubated for 60 min in KRB medium with 30 mmol/l KCl, 250 μmol/l diazoxide, 2 or 16 mmol/l glucose, and test agents.

For islet perifusion, batches of 25 islets each were perifused in parallel microchambers (Biovail, Minneapolis, MN) with oxygenated KRB medium with 2 or 16 mmol/l glucose at a rate of 0.8 ml/min, and the fractions of the perfusate were collected once per minute for insulin measurement. For perfusion of dispersed islet cells, ~300 freshly hand-picked islets were washed twice with Ca^{2+}/Mg^{2+}-free PBS and incubated in 300 μl enzyme-free cell dissociation buffer (Cellstripper; Mediatech, Herndon, VA) at room temperature for 3 min with occasional agitation and further dispersed by gentle trituration. Dispersed cells were rinsed in islet culture medium, and aliquots (50 μl) of the cell suspension were transferred to each of three parallel microchambers for perifusion or were used for the measurement of total insulin content. The perifusion procedure for the dispersed cells was the same as for intact islets described above, except that 50 μmol/l of Ro-20-1724 (a phosphodiesterase inhibitor) was added to the KRB medium throughout. Insulin concentration in aliquots of the incubation or perifusion buffers was measured by the ultrasensitive rat insulin ELISA kit from ALPCO Diagnostics (Windham, NH).

Statistical analysis. Experimental values are given as means ± SE. Single-factor ANOVA was used to compare mean values between groups in the GSIS experiments.

RESULTS

To assess the contribution of $K_V2.1$ to the β-cell I_{DR}, 85 venoms were screened in a functional $^{86}Rb^+$ efflux assay using a stable CHO.$K_V2.1$ cell line. Venom from the tarantula, *Plesiophrictus guangxiensis* sp. nov., was found to display the highest inhibitory potency and was fractionated by HPLC. The most active purified fraction, GxTX-1, was sequenced and found to consist of two variants, 65% GxTX-1E and 35% GxTX-1D, that only differ at the NH_2-terminal residue, glutamate or aspartate, respectively (Table 1). A small inactive peak that elutes separately from GxTX-1 is present in the native purified sample (Fig. 1*A*). Such behavior has also been observed in the separation of HaTX (28). A second less-active fraction, GxTX-2, was also sequenced. GxTX-2 is related to the $K_V2.1$ gating-modifier peptides, HaTX, ScTx1, and SGTx (28–30). GxTX-1 exhibits very little sequence identity with any of these peptides but is related to the gating-modifier peptides, Jingzhaotoxin-III (31), GsMTx-4 (32), and VSTX1 (33), peptidyl tarantula venom inhibitors of sodium, nonselective stretch, and the bacterial K^+ channel K_VAP, respectively (Table 1).

To confirm the identity of the purified peptides and because of their low abundance in the native venom, both GxTX-1E and GxTX-1D were produced by solid-phase synthesis. Folded GxTX-1E coelutes with native peptide in reverse-phase HPLC (Fig. 1). GxTX-1D shows identical chromatographic behavior (not shown). In the $^{86}Rb^+$ efflux assay, GxTX-1E is a slightly more potent $K_V2.1$ inhibitor than the purified native mixture and GxTX-1D (half-maximal concentration [IC_{50}] values of 0.71, 1.5, and 1.8 nmol/l, respectively; $n = 2$) (Fig. 1*B*), suggesting that synthetic GxTX-1 has similar characteristics to native peptide. Because of the advantage of being able to produce large quantities of biologically active peptide, synthetic GxTX-1E was further characterized and used to probe the role of I_{DR} in β-cells.

GxTX-1E is a gating-modifier peptide. Inhibition of $K_V2.1$ by GxTX-1E was characterized by whole-cell voltage-clamp electrophysiology. GxTX-1E (43 nmol/l) inhibited the current in CHO.h$K_V2.1$ cells at both +20 mV and +80 mV (Fig. 2*A–C*). At +20 mV, 43 nmol/l GxTX-1E inhibited CHO.h$K_V2.1$ current 98 ± 1% ($n = 5$). The current-voltage relation shows that GxTX-1E shifts the voltage-dependence of h$K_V2.1$ channel activation, a hallmark feature of gating-modifier peptides (Fig. 2*D*). Using IonWorks automated electrophysiology, K_D values for inhibition of $K_V2.1$ by GxTX-1E were estimated from fits to a single (2.6 nmol/l; Fig. 2*E*, dashed line; average values of 2.0 ± 0.4 nmol/l [$n = 4$]) or a four-equivalent-site model (15.1 nmol/l; Fig. 2*E*, solid line; average 12.0 ± 1.4 nmol/l [$n = 4$]) (25). The potency of GxTX-1E on h$K_V2.1$ channels expressed in *Xenopus* oocytes was 5.1 ± 0.4 nmol/l ($n = 3$) using a single-site model (not shown). GxTX-1E inhibited $K_V2.2$ channels with similar potency (K_D of 2.6 ± 0.4 nmol/l, $n = 3$) as $K_V2.1$ when tested by IonWorks automated electrophysiology (Fig. 2*F*) and also shifted the voltage dependence of $K_V2.2$ channel opening (not shown).

GxTX-1E selectivity for $K_V2.1/K_V2.2$ channels. GxTX-1E was tested at 4 μmol/l, 1,000-fold above its IC_{50} for $K_V2.1$, against a variety of ion channels. Using Ion-

Downloaded from http://diabetesjournals.org/diabetes/article-pdf/55/4/1034/383688/zdb00406001034.pdf by guest on 24 February 2022

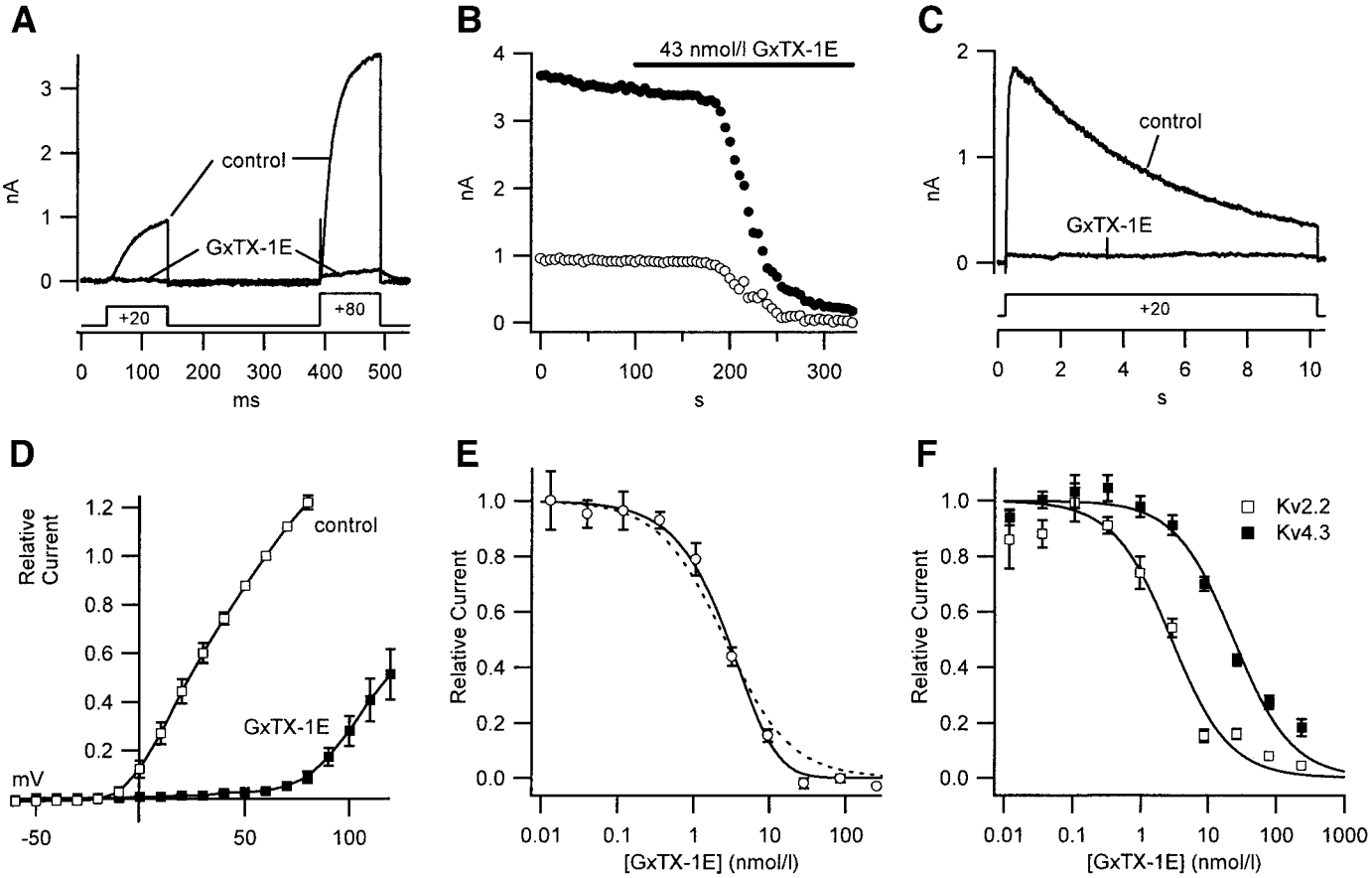

FIG. 2. Inhibition of CHO.hK$_V$2.1 channels by GxTX-1E. *A*: Membrane currents before and after application of 43 nmol/l GxTX-1E. *B*: Current amplitude at +20 (○) and +80 (●) mV plotted versus time. *C*: Membrane current activated by 10 s steps for the same cell as in *A*. *D*: Plot of relative current versus voltage before and after the addition of 43 nmol/l GxTX-1E. *E*: GxTX-1E inhibition of hK$_V$2.1 measured by IonWorks. Solid and dashed lines represent the fit of a four-equivalent and single-site model, respectively. *F*: GxTX-1E inhibition of hK$_V$2.2 and hK$_V$4.3 measured by IonWorks. Lines are fits of a single-site model.

Works automated electrophysiology, GxTX-1E had no significant effect on K$_V$1.2, K$_V$1.3, K$_V$1.5, or K$_V$3.2 channels. However, as observed with HaTX (28) and ScTx1 (29), GxTX-1E inhibited K$_V$4.3 channels with IC$_{50}$s of 24 (Fig. 2*F*) and 54 nmol/l in two experiments. Thus, GxTX-1E is at least eightfold weaker on K$_V$4.3 as compared with K$_V$2 channels. Because K$_V$4 channels produce a rapidly inactivating A-type current, they are not expected to be related to the slowly inactivating I$_{DR}$. In other assays, GxTX-1E had no significant activity against the high-conductance, calcium-activated K$^+$ channel, the calcium channels Ca$_v$1.2 and Ca$_v$2.2, or the sodium channels Na$_v$1.5, Na$_v$1.7, and Na$_v$1.8. Therefore, GxTX-1E is an appropriate probe for studying the contribution of K$_V$2 channels to the β-cell I$_{DR}$.

GxTX-1E inhibits the delayed rectifier of mouse β-cells. Similar to hK$_V$2.1 channels, I$_{DR}$ of mouse β-cells inactivates slowly and is inhibited by GxTX-1E (Fig. 3*A*–*C*). When measured at +20 mV, 43 nmol/l GxTX-1E inhibited I$_{DR}$ of mouse β-cells by 89 ± 3% (n = 11). As seen with hK$_V$2.1, the inhibition of I$_{DR}$ by GxTX-1E is less prominent at more positive voltages (Fig. 3*D*). However, at greater depolarizations, significant differences were seen between the interaction of GxTX-1E with the β-cell current and hK$_V$2.1. At +80 mV, the fraction of mouse β-cell I$_{DR}$ blocked by 43 nmol/l GxTX-1E was 57 ± 3% (n = 11) compared with 93 ± 2% for hK$_V$2.1 channels (Fig. 3*E*). In addition, the potency of the nonselective K$^+$ channel blocker TEA is greater on the β-cell I$_{DR}$ (IC$_{50}$ 2.2 mmol/l) than on hK$_V$2.1 expressed in *Xenopus* oocytes (IC$_{50}$ 8.2 mmol) (Fig. 3*F*). The potency of TEA block of hK$_V$2.1 channels was confirmed with CHO.K$_V$2.1 cells (IC$_{50}$ 9.3 mmol/l; not shown).

Mouse β-cell action potentials are broadened by application of GxTX-1E. Consistent with the idea that the β-cell I$_{DR}$ is involved in action potential repolarization (10), GxTX-1E broadened glucose-induced action potentials in mouse β-cells (Fig. 4*A*–*C*). In contrast to previous reports where a nonselective K$^+$ channel inhibitor, TEA, was used (34), the selectivity of GxTX-1E confirms that action potential broadening in the presence of high glucose occurs through inhibition of I$_{DR}$ alone. To measure the effect of GxTX-1E on action potential repolarization more systematically, we evoked action potentials by depolarizing current injection (Fig. 4*D*). GxTX-1E slowed the rate (dV/dt) of action potential repolarization by 53 ± 7% (n = 4) and increased action potential duration by 30 ± 6% (n = 4; measured at half height). GxTX-1E had no effect on the resting membrane potential of β-cells in low glucose (not shown), unlike inhibitors of K$_{ATP}$ channels.

GxTX-1E enhances glucose-stimulated [Ca^{2+}]$_i$ oscillations. Prolongation of the action potential by inhibition of I$_{DR}$ should result in increased [Ca^{2+}]$_i$ in response to elevated glucose. We tested this idea by measuring changes in [Ca^{2+}]$_i$ oscillations in dissociated β-cells using fura-2 imaging. Glucose at 8 mmol/l was optimal for

Downloaded from http://diabetesjournals.org/diabetes/article-pdf/55/4/1034/383688/zdb00406001034.pdf by guest on 24 February 2022

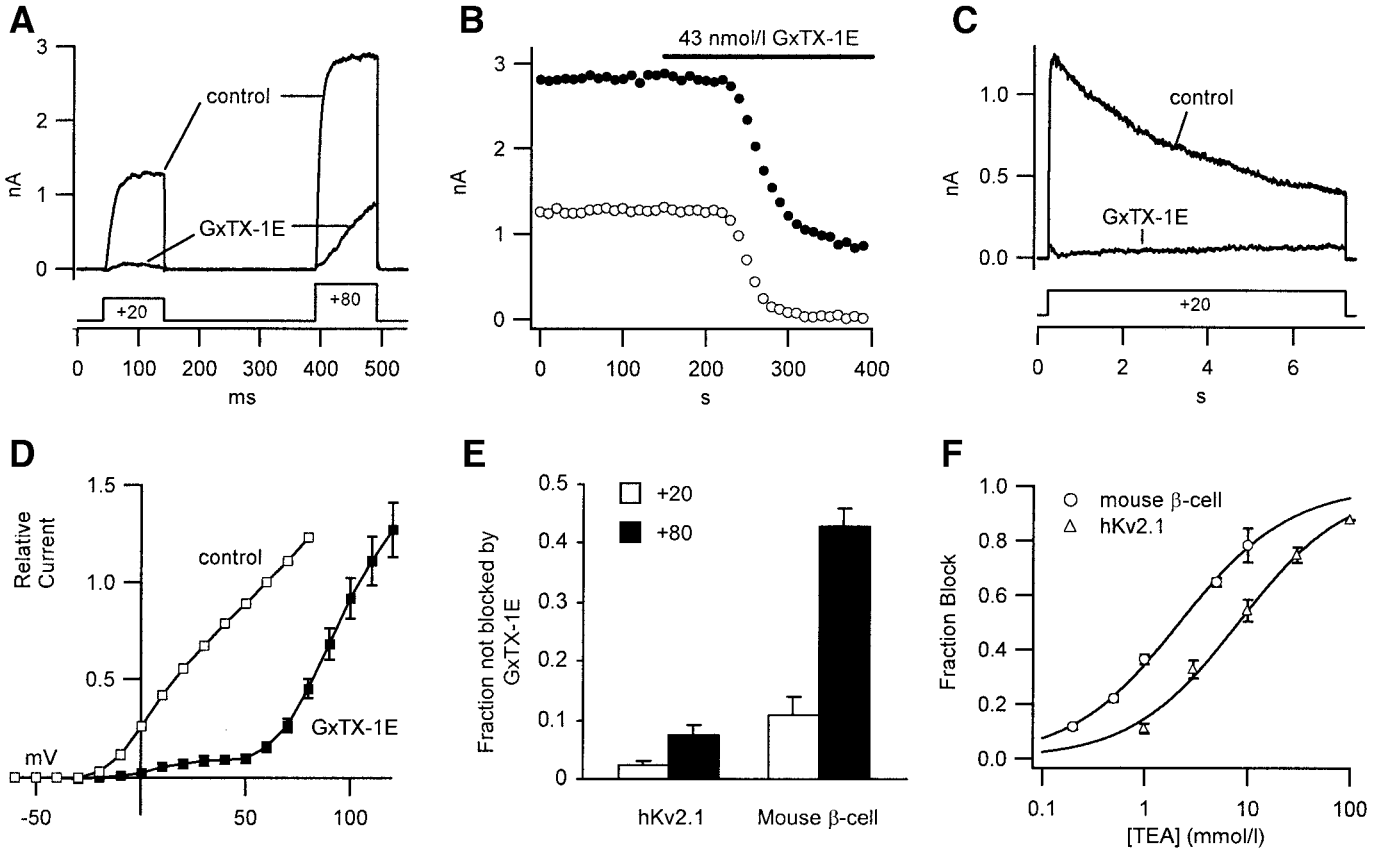

FIG. 3. Inhibition of I_{DR} of mouse β-cells by GxTX-1E. *A–D*: Experimental procedures were the same as in Fig. 2. *E*: Fraction of unblocked current in 43 nmol/l GxTX-1E at +20 (○) and +80 (●) mV for CHO.hK_V2.1 channels and mouse β-cell I_{DR}. *F*: Dose-dependence of TEA block of the mouse β-cell I_{DR} and hK_V2.1 expressed in *Xenopus* oocytes measured at +20 mV.

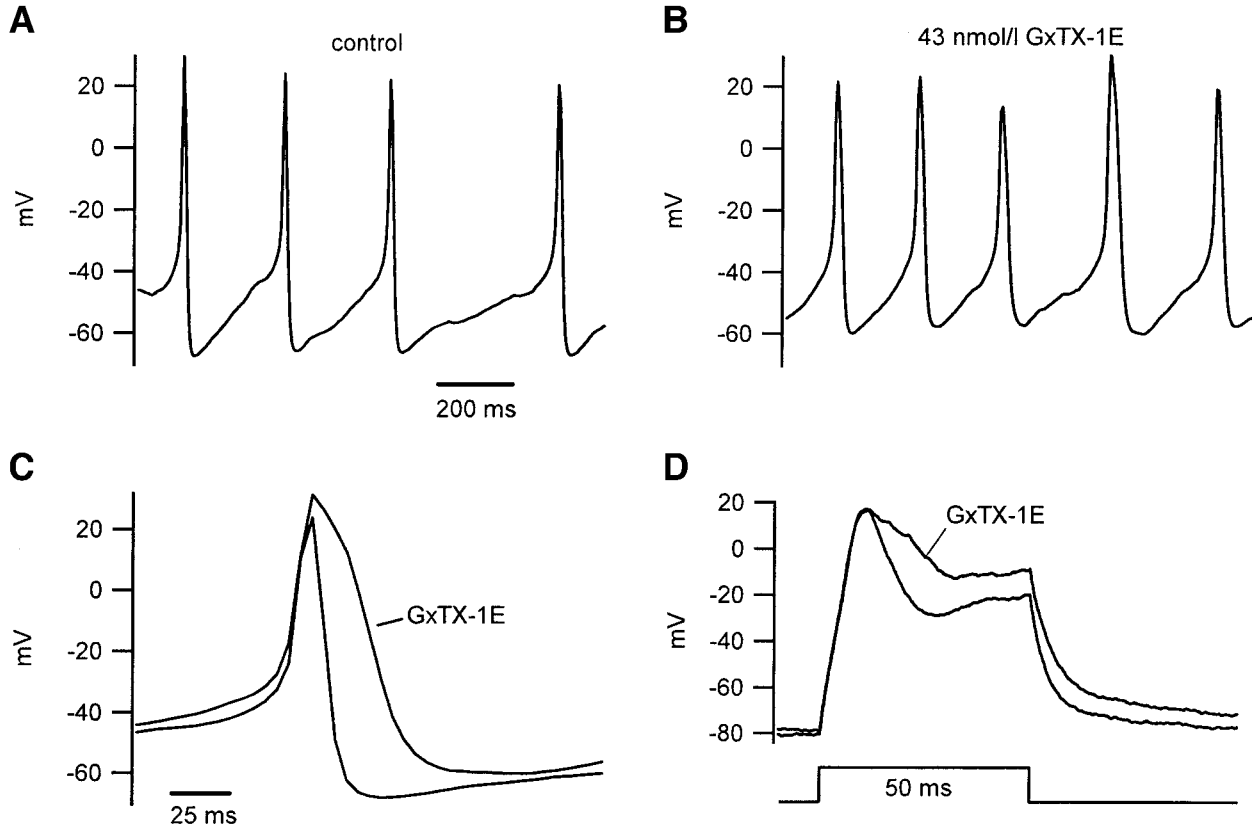

FIG. 4. GxTX-1E broadens the β-cell action potential. *A* and *B*: Action potentials induced by 10 mmol/l glucose were recorded before (*A*) and after (*B*) the addition of 43 nmol/l GxTX-1E. *C*: Representative action potentials from *A* and *B* are aligned at the peak to illustrate action potential broadening by GxTX-1E. *D*: Action potentials triggered by injection of positive current (100 pA) before and after the addition of 100 nmol/l GxTX-1E.

Downloaded from http://diabetesjournals.org/diabetes/article-pdf/55/4/1034/383688/zdb00406001034.pdf by guest on 24 February 2022

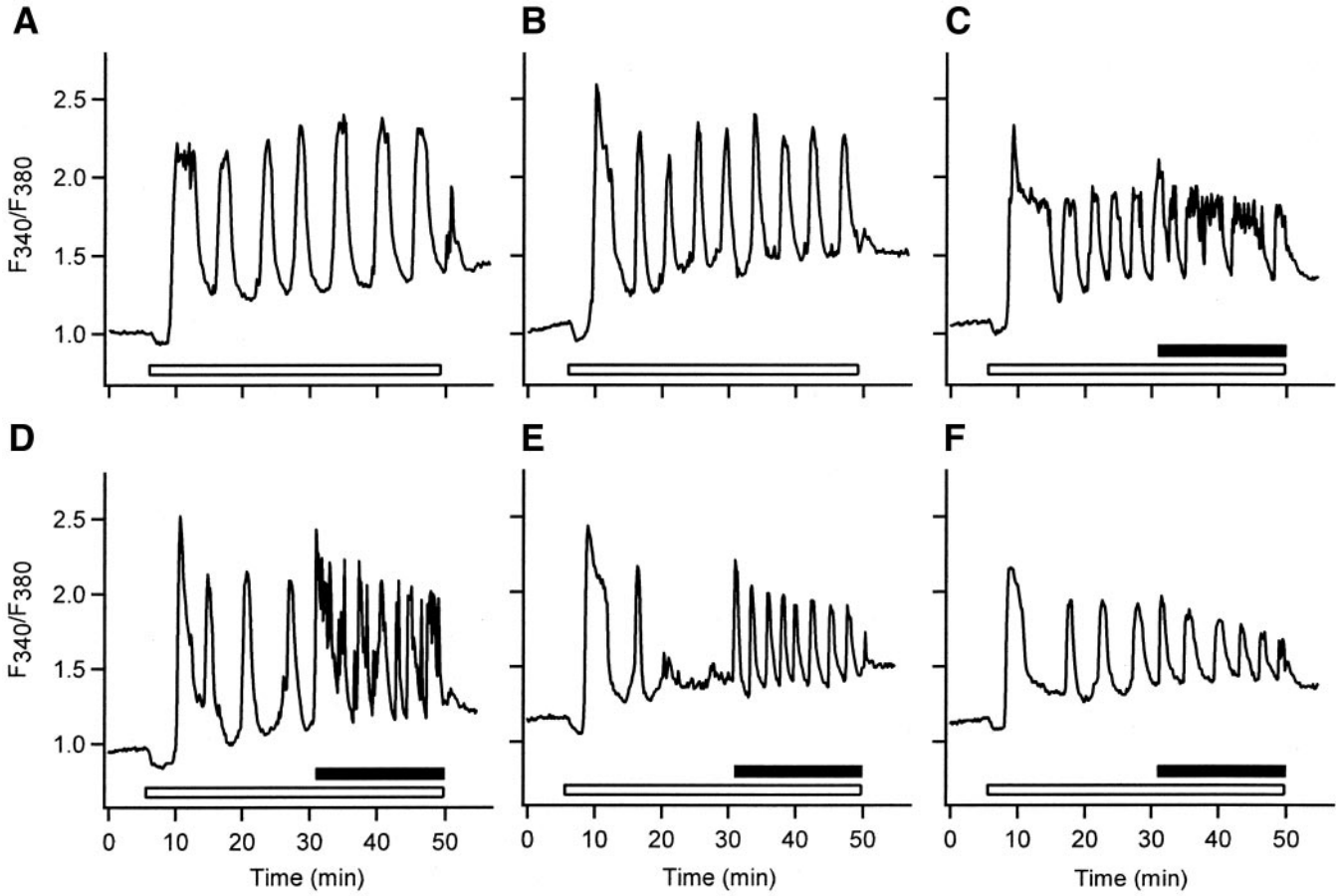

FIG. 5. GxTX-1E augments glucose-stimulated $[Ca^{2+}]_i$ oscillations. *A–F*: Plots of the fluorescence intensity ratio of fura-2 (F340/F380) in single mouse islet cells versus time. The periods of application of 8 mmol/l glucose and 43 nmol/l GxTX-1E are denoted by open and solid bars, respectively. Cells were perfused with 3 mmol/l glucose at all other times. *A–B* and *C–F* are separate experiments.

inducing $[Ca^{2+}]_i$ oscillations that were stable for nearly 1 h (Fig. 5*A* and *B*). For example, when the area under the curve is measured from 15 to 30 min and from 30 to 45 min for the cells in Fig. 5*A* and *B*, $[Ca^{2+}]_i$ rose only 3 and 10%, respectively, between these time periods. On average, $[Ca^{2+}]_i$ increased 9 ± 4% (n = 27) over this time. We then asked if inhibition of I_{DR} by GxTX-1E would enhance $[Ca^{2+}]_i$. GxTX-1E (43 nmol/l) was added to the bath after ~15 min of stable $[Ca^{2+}]_i$ oscillations. Figure 5*C–F* shows examples of individual cells from a single experiment and demonstrates the types of responses seen after exposure to GxTX-1E. In some cells, the oscillations became broader (Fig. 5*C*), while in others the frequency increased (Fig. 5*D*). In some cells, GxTX-1E restored oscillations that had stopped (Fig. 5*E*), while in others GxTX-1E had only a modest effect (Fig. 5*F*). On average, GxTX-1E produced a 38 ± 5% (n = 61) increase in $[Ca^{2+}]_i$ relative to the period before GxTX-1E addition. Importantly, GxTX-1E had no effect on $[Ca^{2+}]_i$ when applied in low (3 mmol/l) glucose (not shown), and the enhanced $[Ca^{2+}]_i$ oscillations produced by GxTX-1E in 8 mmol/l glucose were rapidly terminated upon lowering of glucose (Fig. 5*C–F*).

GSIS is enhanced by GxTX-1E. The findings that GxTX-1E is an effective inhibitor of the β-cell I_{DR} and enhances glucose-dependent Ca^{2+} oscillations suggest that it should augment GSIS. As expected, insulin secretion at 16 mmol/l glucose was enhanced 3.5-fold by 2 μmol/l GxTX-1E when tested in a static assay (Fig. 6*A*; $P <$ 0.001). TEA (10 mmol/l) enhanced GSIS twofold (Fig. 6*A*; $P < 0.01$). These effects on insulin secretion were glucose dependent, since neither GxTX-1E nor TEA had an effect at 2 mmol/l glucose. As a positive control, 10 nmol/l GLP-1 enhanced GSIS by fivefold ($P < 0.001$). The enhancement of GSIS by GxTX-1E was also observed in perifusion studies of mouse islets. The addition of GxTX (1 μmol/l) to the perifusate with 16 mmol/l glucose doubled the rate of insulin secretion (average insulin concentration 2.1 ± 0.5 ng/ml) compared with perifusion in glucose alone (1.1 ± 0.2 ng/ml) (Fig. 6*B*).

Addition of TEA after a 20-min wash of GxTX resulted in additional enhancement over the GxTX-enhanced signal (Fig. 6*B*, P = 0.060). Since recovery from GxTX-1E inhibition of $hK_V2.1$ is slow (off time constant [τ_{off}] ~28 min; not shown), the effect of TEA in these experiments may be due to both TEA and the residual effects of GxTX-1E. The additional enhancement produced by TEA may also arise from the action of TEA on other channels besides K_V channels.

In separate static assays of intact islets, GxTX-1E was found to have an EC_{50} of 400 nmol/l for the enhancement of GSIS (n = 2, not shown). However, in dispersed islet cells, GxTX-1E was more potent (Fig. 6*C*) than it is in intact islets. Both 50 nmol/l and 1 μmol/l GxTX-1E exhibited a significant enhancement over 16 mmol/l glucose alone (average [10–20 min] respective % insulin content/min 0.54 ± 0.07, 0.48 ± 0.05, and 0.31 ± 0.04, $P < 0.05$), and were not significantly different from each other.

Downloaded from http://diabetesjournals.org/diabetes/article-pdf/55/4/1034/383688/zdb00406001034.pdf by guest on 24 February 2022

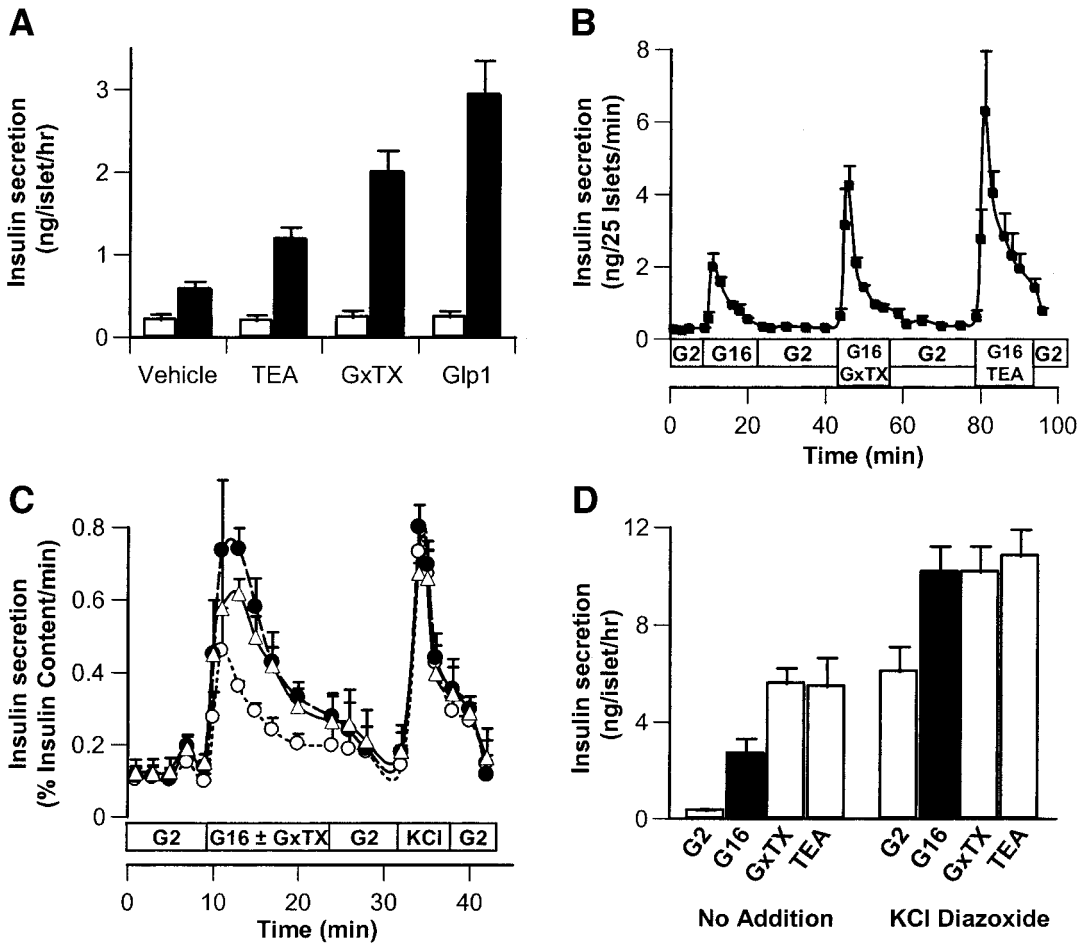

FIG. 6. Effect of GxTX-1E on GSIS. *A*: Static incubation of mouse islets for 1 h with either 2 (□) or 16 (■) mmol/l glucose in the presence or absence of 10 mmol/l TEA, 2 μmol/l GxTX-1E, or 10 nmol/l GLP-1 (n = 12). *B*: Perifusion of islets with either 2 (G2) or 16 (G16) mmol/l glucose (n = 3). GxTX-1E (1 μmol/l) and TEA (5 mmol/l) were added to the perifusate at indicated times. *C*: Perifusion of dispersed islet cells with 16 mmol/l glucose (○), 50 nmol/l GxTX-1E (●), or 1 μmol/l GxTX-1E (△) (n = 4). After washout in 2 mmol/l glucose, all samples were treated with 30 mmol/l KCl in 2 mmol/l glucose. *D*: Insulin secretion in the absence (no addition) or presence of 30 mmol/l KCl and 250 μmol/l diazoxide (K_{ATP} channel independent) (n = 4). Test groups were (from *left* to *right*) 2 mmol/l glucose, 16 mmol/l glucose, and 16 mmol/l glucose in the presence of 1 μmol/l GxTX-1E or 5 mmol/l TEA.

The enhancement of GSIS by GxTX-1E was not due to effects on the K_{ATP} channel–independent pathway, as shown in Fig. 6*D*. In the presence of elevated KCl (30 mmol/l) to depolarize the plasma membrane and diazoxide (250 μmol/l) to maintain K_{ATP} channels in the open state, insulin secretion was significantly higher at 16 than at 2 mmol/l glucose (10.2 vs. 6.1 ng · islet^{-1} · h^{-1}, n = 4, P = 0.01), but neither 1 μmol/l GxTX-1E nor 5 mmol/l TEA caused additional insulin release. Note that in the controls, GxTX-1E and TEA repeated their enhancement of insulin secretion over that at 16 mmol/l glucose ($P < 0.05$). Taken together, these data point to a mechanism for specific enhancement of insulin secretion at elevated glucose levels by blocking the β-cell I_{DR}.

DISCUSSION

In this study, we report the identification, purification, primary sequence determination, synthesis, and use of GxTX-1, a potent inhibitor of the β-cell I_{DR}. GxTX-1 broadens β-cell action potentials, increases calcium oscillations, and enhances GSIS. GxTX-1 inhibits 90% of the β-cell I_{DR}, making it a suitable probe for the physiological role of the I_{DR}. GxTX-1 broadens the glucose-induced action potential but has no effect on the resting potential in low glucose. Similarly, GxTX-1 augments glucose-dependent calcium oscillations without affecting resting $[Ca^{2+}]_i$. Further, the stimulation of insulin secretion by GxTX-1 is strictly glucose dependent, as expected, since I_{DR} is only active at membrane potentials above −20 mV, a depolarization level only seen in elevated glucose. This property, coupled with slow opening kinetics (Fig. 3*A*), makes the I_{DR} ideal for contributing to the repolarization phase of the β-cell action potential. The observation that GxTX-1 has no effect on the K_{ATP} channel–independent pathways suggests that the observed effects of GxTX-1 on insulin secretion are limited to inhibition of I_{DR}.

The concentration (43 nmol/l) at which GxTX-1 broadens action potentials and enhances calcium oscillations and the concentration (50 nmol/l) at which GxTX-1 enhances insulin secretion from dispersed islet cells are consistent with inhibition of the mouse β-cell I_{DR}. However, higher concentrations (EC_{50} ~400 nmol/l) of GxTX-1 were required to enhance GSIS in intact islets, suggesting a more difficult access of the peptide to the core of the islets as compared with dispersed single β-cells. A similar scenario has been suggested to explain the effects of HaTX on calcium oscillations in whole islets (15). Nonetheless, the effects of GxTX-1 taken together are consistent with

Downloaded from http://diabetesjournals.org/diabetes/article-pdf/55/4/1034/383688/zdb00406001034.pdf by guest on 24 February 2022

the hypothesis that GxTX-1 enhances insulin secretion from mouse islets through inhibition of the β-cell I_{DR}.

Identity of the delayed-rectifier channels in mouse β-cells. Selectivity studies with GxTX-1 suggest that the major, GxTX-1–sensitive component of the β-cell I_{DR} contains K_V2 subunits. The only other channel we identified that is blocked by GxTX-1 is $K_V4.3$, which is not likely to contribute significantly to the β-cell I_{DR}, since it is neither expressed in mouse β-cells (13) nor found in human islets by PCR (35). In addition, K_V4 channels normally produce a rapidly inactivating current, distinct from the slowly inactivating I_{DR} of β-cells.

Of the two known K_V2 family members, $K_V2.1$ is the best candidate to encode I_{DR}. $K_V2.1$ is expressed at high levels in islets from various species (8,12), and immunohistochemical analysis indicates that expression of $K_V2.1$ in primate islets is restricted to β-cells (35). The other member of the K_V2 family, $K_V2.2$, appears to be specifically located in δ-cells of primate islets (35) and is not found in rat islets (8).

Although block of the β-cell I_{DR} suggests the presence of $K_V2.1$, clear differences between the mouse β-cell I_{DR} and $hK_V2.1$ were observed. The GxTX-1–induced shift in voltage-dependent channel opening was greater for $hK_V2.1$ than for mouse β-cell I_{DR}, and mouse β-cell I_{DR} is more sensitive to TEA than $hK_V2.1$ (Fig. 3*F*). These pharmacological differences are not likely due to species differences. The sequences of mouse and human $K_V2.1$ are nearly identical, and sequence identity is 100% in the regions where gating modifiers and TEA are thought to bind. Indeed, the I_{DR} of human β-cells is also more sensitive to TEA (IC_{50} 0.54 mmol/l) (9) than $hK_V2.1$. The pharmacological differences between native and heterologously expressed channels may be due to posttranslational modification, association of unknown accessory subunits, or heterotetramerization of α subunits. Gating modifier peptides, unlike pore blockers, bind to the channel with a stoichiometry of 4:1, and the number of inhibitor molecules bound determines the amplitude of the shift in channel gating (25). Coassembly of $K_V2.1$ subunits with GxTX-1–insensitive, TEA-sensitive subunits, might result in a pharmacological profile similar to that of the I_{DR} of β-cells.

In this study, we have shown that GxTX-1 is a novel and suitable tool to probe the role of the β-cell I_{DR} in insulin secretion and to investigate the molecular composition of the β-cell I_{DR}. The glucose dependence of the effects of GxTX-1 on both $[Ca^{2+}]_i$ oscillations and insulin release predict that a blocker of I_{DR}, unlike K_{ATP} channel blockers, should not induce hypoglycemia and may represent an improved approach for the treatment of type 2 diabetes. Lastly, the availability of biologically active synthetic GxTX-1 should facilitate studies of the mechanisms that control insulin secretion.

ACKNOWLEDGMENTS

The authors thank John P. Felix, Kevin Ratliff, William Schmalhofer, Brande Williams, and Dr. Lizhen Yan for assistance in technical aspects and/or discussion of this manuscript.

REFERENCES

1. Henquin J-C: Triggering and amplifying pathways of regulation of insulin secretion by glucose. *Diabetes* 49:1751–1760, 2000
2. Ashcroft FM, Rorsman P: Electrophysiology of the pancreatic beta-cell. *Prog Biophys Mol Biol* 54:87–143, 1989
3. Rendell M: The role of sulphonylureas in the management of type 2 diabetes mellitus. *Drugs* 64:1339–1358, 2004
4. Tabcharani JA, Misler S: Ca^{2+}-activated K^+ channel in rat pancreatic islet B cells: permeation, gating and blockade by cations. *Biochim Biophys Acta* 982:62–72, 1989
5. Gopel SO, Kanno T, Barg S, Eliasson L, Galvanovskis J, Renstrom E, Rorsman P: Activation of $Ca(^{2+})$-dependent $K(^+)$ channels contributes to rhythmic firing of action potentials in mouse pancreatic beta cells. *J Gen Physiol* 114:759–770, 1999
6. Zhang M, Houamed K, Kupershmidt S, Roden D, Satin L: Pharmacological properties and functional role of K_{slow} current in mouse pancreatic β-cells: SK channels contribute to K_{slow} tail current and modulate insulin secretion. *J Gen Physiol* 126:353–363, 2005
7. Gopel SO, Kanno T, Barg S, Rorsman P: Patch-clamp characterisation of somatostatin-secreting δ-cells in intact mouse pancreatic islets. *J Physiol* 528:497–507, 2000
8. MacDonald PE, Sewing S, Wang J, Joseph JW, Smukler SR, Sakellaropoulos G, Saleh MC, Chan CB, Tsushima RG, Salapatek AM, Wheeler MB: Inhibition of $K_v2.1$ voltage-dependent K^+ channels in pancreatic beta-cells enhances glucose-dependent insulin secretion. *J Biol Chem* 277:44938–44945, 2002
9. Herrington J, Sanchez M, Wunderler D, Yan L, Bugianesi RM, Dick IE, Clark SA, Brochu RM, Priest BT, Kohler MG, McManus OB: Biophysical and pharmacological properties of the voltage-gated potassium current of human pancreatic β-cells. *J Physiol* 567:159–175, 2005
10. Smith PA, Bokvist K, Arkhammar P, Berggren PO, Rorsman P: Delayed rectifying and calcium-activated K^+ channels and their significance for action potential repolarization in mouse pancreatic beta-cells. *J Gen Physiol* 95:1041–1059, 1990
11. Henquin JC: Tetraethylammonium potentiation of insulin release and inhibition of rubidium efflux in pancreatic islets. *Biochem Biophys Res Commun* 77:551–556, 1977
12. MacDonald PE, Ha XF, Wang J, Smukler SR, Sun AM, Gaisano HY, Salapatek AM, Backx PH, Wheeler MB: Members of the K_v1 and K_v2 voltage-dependent $K(^+)$ channel families regulate insulin secretion. *Mol Endocrinol* 15:1423–1435, 2001
13. Roe MW, Worley JF 3rd, Mittal AA, Kuznetsov A, DasGupta S, Mertz RJ, Witherspoon SM, 3rd, Blair N, Lancaster ME, McIntyre MS, Shehee WR, Dukes ID, Philipson LH: Expression and function of pancreatic beta-cell delayed rectifier K^+ channels: role in stimulus-secretion coupling. *J Biol Chem* 271:32241–32246, 1996
14. Tamarina NA, Kuznetsov A, Dukes I, Philipson LH: Delayed rectifier potassium channel $K_v2.1$ role in β-cell physiology and insulin secretion (Abstract). *Diabetes* 51 (Suppl. 2):A372, 2002
15. Tamarina NA, Kuznetsov A, Fridlyand LE, Philipson LH: Delayed-rectifier ($K_v2.1$) regulation of pancreatic β-cell calcium responses to glucose: inhibitor specificity and modeling. *Am J Physiol Endocrinol Metab* 289: E578–E585, 2005
16. Yin CM, Tan Y: One new species of the genus *Plesiophrictus* from south China (Araneae: Theraphosidae). *Life Science Research (Hunan Normal University, China)* 4:151–154, 2000
17. Middleton RE, Warren VA, Kraus RL, Hwang JC, Liu CJ, Dai G, Brochu RM, Kohler MG, Gao YD, Garsky VM, Bogusky MJ, Mehl JT, Cohen CJ, Smith MM: Two tarantula peptides inhibit activation of multiple sodium channels. *Biochemistry* 41:14734–14747, 2002
18. Garsky VM, Lumma PK, Freidinger RM, Smith MM, Cohen CJ: The total synthesis of μ-Agatoxin-IV: a spider toxin selective for insect Na channels. In *Peptides*. Maia HLS, Ed. Leiden, ESCOM Science Publishers B.V., 1995, p. 375–376
19. Gasteiger E, Hoogland C, Gattiker A, Duvaud S, Wilkins MR, Appel RD, Bairoch A: Protein identification and analysis tools on the ExPASy server. In *The Proteomics Protocols Handbook*. Walker JM, Ed. Totowa, NJ, Humana Press, 2005, p. 571–607
20. Gill SC, von Hippel PH: Calculation of protein extinction coefficients from amino acid sequence data. *Anal Biochem* 182:319–326, 1989
21. Yan L, Herrington J, Goldberg E, Dulski PM, Bugianesi RM, Slaughter RS, Banerjee P, Brochu RM, Priest BT, Kaczorowski GJ, Rudy B, Garcia ML: *Stichodactyla helianthus* peptide, a pharmacological tool for studying $K_v3.2$ channels. *Mol Pharmacol* 67:1513–1521, 2005
22. Hamill OP, Marty A, Neher E, Sakmann B, Sigworth FJ: Improved patch-clamp techniques for high-resolution current recording from cells and cell-free membrane patches. *Pflugers Arch* 391:85–100, 1981
23. Arena JP, Liu KK, Paress PS, Cully DF: Avermectin-sensitive chloride currents induced by *Caenorhabditis elegans* RNA in Xenopus oocytes. *Mol Pharmacol* 40:368–374, 1991

Downloaded from http://diabetesjournals.org/diabetes/article-pdf/55/4/1034/383688/zdb00406001034.pdf by guest on 24 February 2022

24. Kiss L, Bennett PB, Uebele VN, Koblan KS, Kane SA, Neagle B, Schroeder K: High throughput ion-channel pharmacology: planar-array-based voltage clamp. *Assay Drug Dev Technol* 1:127–135, 2003
25. Swartz KJ, MacKinnon R: Hanatoxin modifies the gating of a voltage-dependent K^+ channel through multiple binding sites. *Neuron* 18:665–673, 1997
26. Lacy PE, Kostianovsky M: Method for the isolation of intact islets of Langerhans from the rat pancreas. *Diabetes* 16:35–39, 1967
27. Zhou YP, Marlen K, Palma JF, Schweitzer A, Reilly L, Gregoire FM, Xu GG, Blume JE, Johnson JD: Overexpression of repressive cAMP response element modulators in high glucose and fatty acid-treated rat islets: a common mechanism for glucose toxicity and lipotoxicity? *J Biol Chem* 278:51316–51323, 2003
28. Swartz KJ, MacKinnon R: An inhibitor of the $K_V2.1$ potassium channel isolated from the venom of a Chilean tarantula. *Neuron* 15:941–949, 1995
29. Escoubas P, Diochot S, Celerier ML, Nakajima T, Lazdunski M: Novel tarantula toxins for subtypes of voltage-dependent potassium channels in the K_V2 and K_V4 subfamilies. *Mol Pharmacol* 62:48–57, 2002
30. Lee CW, Kim S, Roh SH, Endoh H, Kodera Y, Maeda T, Kohno T, Wang JM, Swartz KJ, Kim JI: Solution structure and functional characterization of SGTx1, a modifier of $K_V2.1$ channel gating. *Biochemistry* 43:890–897, 2004
31. Xiao Y, Tang J, Yang Y, Wang M, Hu W, Xie J, Zeng X, Liang S: Jingzhaotoxin-III, a novel spider toxin inhibiting activation of voltage-gated sodium channel in rat cardiac myocytes. *J Biol Chem* 279:26220–26226, 2004
32. Suchyna TM, Johnson JH, Hamer K, Leykam JF, Gage DA, Clemo HF, Baumgarten CM, Sachs F: Identification of a peptide toxin from Grammostola spatulata spider venom that blocks cation-selective stretch-activated channels. *J Gen Physiol* 115:583–598, 2000
33. Ruta V, Jiang Y, Lee A, Chen J, MacKinnon R: Functional analysis of an archaebacterial voltage-dependent K^+ channel. *Nature* 422:180–185, 2003
34. Atwater I, Ribalet B, Rojas E: Mouse pancreatic beta-cells: tetraethylammonium blockage of the potassium permeability increase induced by depolarization. *J Physiol* 288:561–574, 1979
35. Yan L, Figueroa DJ, Austin CP, Liu Y, Bugianesi RM, Slaughter RS, Kaczorowski GJ, Kohler MG: Expression of voltage-gated potassium channels in human and rhesus pancreatic islets. *Diabetes* 53:597–607, 2004

Downloaded from http://diabetesjournals.org/diabetes/article-pdf/55/4/1034/383688/zdb00406001034.pdf by guest on 24 February 2022